A three dimensional infinite wedge shaped solid block sliding into water along an inclined beach

S.L. Sun[1], S.Y. Sun[2], G.X. Wu[1,3,*]

[1]College of Shipbuilding Engineering, Harbin Engineering University, Harbin 150001, China

[2]School of Naval Architecture and Ocean Engineering, Jiangsu University of Science and Technology, Zhenjiang 212003, China

[3]Permanent address: Department of Mechanical Engineering, University College London, Torrington Place, London WC1E 7JE, UK

Abstract: The three dimensional (3D) problem of a solid block sliding into water along an inclined beach is investigated. The main part of the block is an infinite wedge cylinder and the front of the body is part of an elliptical cone. Incompressible velocity potential theory is used together with fully nonlinear boundary conditions. When gravity is ignored, it is found that self-similar solution is possible. The boundary element method is used to solve the problem. The free surface shape is updated together with the potential on the free surface until the flow has become self-similar. Convergence studies are taken with respect to marching step and element size. Simulations are made for different bodies and different beach angles. Extensive results are provided for the pressure as well as the free surface shape, and their implications in physics are discussed.

Key words: 3D sliding block; Impact with liquid; Velocity potential theory; Fully nonlinear boundary conditions; Boundary element method.

1. Introduction

A wave generated by the land movement is always of great interest in nature and engineering. At an extreme level, tsunami can be caused by landslide (Synolakis et al., 1997). The problem in this context has been investigated by Liu et al. (2005) through experiments and numerical simulations. At a less dramatic and local level, wave generated by a sliding solid block can also be seen when a newly built ship, or a sailing boat, or a rescue boat is launched into the water, during which accidence can occur. Another example is when an ice block breaks from an iceberg and slides into the sea. This is becoming more and more a concern as more ships are passing though the North Pole. In particular a 'blue' Arctic Ocean is predicted to occur in the summer time from the middle of this century (Hong, 2012) and some new Trans-Arctic shipping routes may become viable (Smith and Stephenson, 2013). A further example is the impulsive wave in reservoir created by the sliding mass (Zweifel et al., 2006).

The work done by Liu et al. (2005) focused on the wave runup and rundown during a 3D mass sliding into water. In addition to the experiment, they undertook numerical simulations based on the Navier-Stokes equation together with the large eddy simulation. The mathematical problem was solved using the finite volume method with the volume of fluid method for the free surface tracking. Here we consider a similar problem in different context. Although our 3D body is also a wedge shaped one, the wedge is on the upright position when it slides along a sloping beach, while in Liu et al. (2005) one of the side surfaces of the wedge lies on the beach. Our work here is

undertaken in the context of fluid/structure impact when the body slides into the water. The entry speed U is relatively large or the period of sliding t is rather short, on the basis $t << g/U$. Therefore the acceleration g due to gravity is ignored. About the viscosity, its effect at large speed or large Reynolds number is expected to be confined within the boundary layer. The length scale of the effect is of order $\sqrt{\kappa \cdot t}$, where κ is kinetic viscosity. This is unlikely to be significant when $t << g/U$. Thus the viscosity is also neglected. Subsequently, we will use the incompressible velocity potential theory with the fully nonlinear boundary condition on the instantaneous free surface. The problem at each time step will be solved by the 3D boundary element method. This is similar to the mathematical model and solution procedure in Wu and Sun (2014) and Sun and Wu (2014). It allows us to capture some local results with high resolution.

Two limiting cases in the present analysis are highly relevant to the problems which have been receiving extensive interest. As the sloping beach tends to be vertical, the sliding wedge problem tends to that of two dimensional (2D) wedge entering water. The fully nonlinear solution of such a problem was first obtained by Dobrovol'skaya (1969) who used the function introduced by Wagner (1932) to reduce the problem of water entry of a wedge to a nonlinear integral equation. Zhao and Faltinsen (1993) then solved this problem by the boundary element method in the time domain and provided the details on some of the challenges in numerical solution in this kind of problem. Semenov and Iafrati (2006) considered an asymmetric wedge using the integral hodograph method. The 2D problem in the physical domain is converted into that in the first quadrant of a parameter plan. Integro-differential equations were derived in the parameter plan based on the velocity magnitude and its direction. The method was further extended by Semenov and Wu (2013) for a water wedge impacting with a non-flat surface. The free fall problem of a wedge in three degrees of freedom entering water obliquely was solved by Xu, Duan and Wu (2010) using the boundary element method.

Another limiting case is when the sloping beach tends to be horizontal. In such a case the problem tends to that of the 3D bow wave of a wedge shaped ship front at high speed (due to the fact that the gravity has been ignored). Bow wave is a major contributor to the wave making resistance which can be a significant part of the total drag experienced by a ship (Larsson and Baba, 1996). The flow near the bow can be highly complex. In the early work on the 2D bow wave, Dagan and Tulin (1972) showed that at lower Froude number there is a stagnation point on the body. At large Froude number, a jet will be developed along the body surface. It will then leave body tangentially. After it reaches a peak it will fall back to the main fluid domain. The problem was further considered by Dias and Vanden-Broeck (1993) who allowed the jet to fall into the Riemann second sheet mathematically and therefore there was no secondary impact between the fallen jet and main liquid. This can be viewed as that the jet and main flow are on the two sides of a zero thickness sheet. They occupy the same space but they do not interact directly. Shakeri et al. (2009) investigated divergent ship bow waves experimentally based on the mechanism of the 2D+T theory.

In general, the case considered in the present work is one of the 3D fluid/structure impact problems. For the fully 3D problem, Miloh (1991) solved the problem of a sphere in oblique water entry through the variable separation method in the spherical coordinate system. The free surface was assumed to remain flat and the velocity potential on the free surface was assumed to remain to be zero. Wagner theory has also been used in various 3D problems. Scolan and Korobkin (2001), Korokin and Scolan (2006) considered a blunt-body impact onto the free surface. Moore et al. (2012) solved the problem of the oblique water entry of 3D bodies at small deadrise angles and they gave the leading order pressure on some axisymmetric bodies. For the problem with the fully nonlinear free surface boundary conditions, Sun and Wu (2013a, 2013b) considered the 3D water entry problems using the boundary element method, in which the mesh was regularly regenerated to account for the large deformation of the free surface and the variation of the wetted surface. The information obtained in the old mesh was transferred to the new mesh. Wu and Sun (2014) further considered a 3D problem with a non-fixed body shape. A related 3D problem of a water cone hitting an inclined wall was considered by Sun and Wu (2014). They showed that when the inner angle of the water cone tended to zero while the incoming flow rate remained finite, the result would tend to the steady flow of a water cylinder hitting the wall.

In general, the 3D fluid/structure impact problem is an extremely challenging one. The rapid and large deformation of the fluid boundary makes both analytical and numerical solutions very difficult to be solved. The work discussed above is only for some specific problems and overall the solutions obtained are still very much limited. The present work is another step in this direction. It focuses on a 3D block sliding along an inclined beach. The main body of the 3D block is a wedge cylinder and the sharp edge of this cylinder is replaced by a small elliptical front. It is illustrated that the self-similar solution is possible for such a problem and the self-similar solution is obtained in time domain. As the body slides into water, the liquid will move up along the beach as well as along the body surface. The beach, the wedge and the free surface will merge at a local point where the waterlines on the beach and on the wedge surface will also intersect. The overall deformation of the free surface and variation of the wetted surfaces of the beach and the body are more complex than those in previous works. All these present some new challenges in the numerical techniques adopted. It needs great care in mesh generation and its quality. In particular this has to be ensured during remeshing which is applied regularly to track the highly deformed free surface and continuously varying wetted surfaces of the beach and the body. The self-similar behaviour of the water motion and the pressure has been shown in Section 3. The convergence study with mesh and time step is also undertaken. Various numerical results are then provided and their implications are discussed.

2. Mathematic Model and Numerical Procedures

2.1. Mathematic model

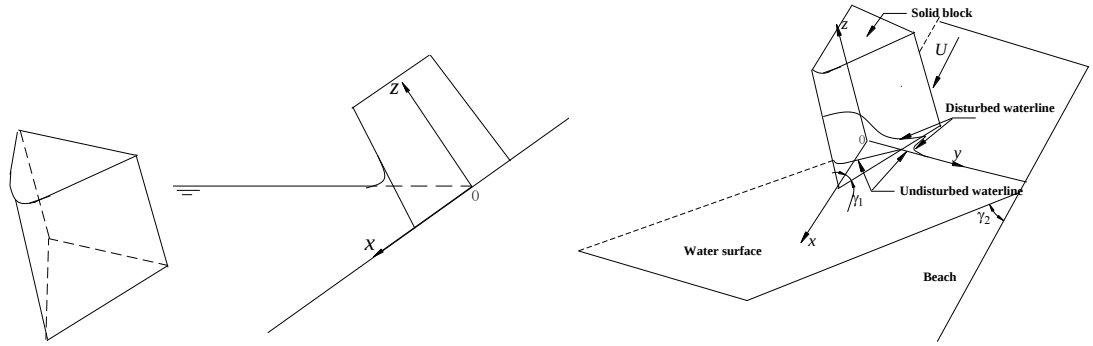

(a) (b) (c)

Fig.1. Sketch of the problem, (a) Full body shape, (b) Side view, (c) Half numerical model.

There has been some work on a 2D wedge sliding into water (Iafrati et al., 2007; Iafrati, 2013). In the present paper, a 3D solid block sliding along a flat inclined beach at constant speed U will be considered and the sketch of the problem is shown in Fig.1. The space-fixed coordinate system $O-xyz$ is defined with x along the direction of the forward speed or the beach, y on the intersection line between the undisturbed free surface and the beach surface and z perpendicular to the beach. When z is a constant, the main part of the cross section of the body is a triangle, or wedge shaped. Based on the potential flow, the velocity at a sharp corner of a solid body can be singular due to discontinuity of normal direction of the body. The effect of this singularity is usually localized. In the problem of 2D water entry of a horizontal wedge, the singular behaviour does not affect the global solution. Principally, it is because the edge of the wedge is fully submerged and is away from the free surface. Here the edge of the wedge would cut through the free surface. Any local singular behaviour would affect the free surface elevation near the edge and the error would propagate into other areas. Thus, the sharp corner $(x \to Ut, y \to 0)$ of the wedge is rounded by part of an ellipse.

We assume that the fluid is inviscid and incompressible and flow irrotational. The velocity potential ϕ can be introduced, which satisfies the Laplace equation in the fluid domain

$$\nabla^2\phi=0 \tag{1}$$

The body which we consider is symmetric about $y=0$ plane. The present problem will be solved in the domain with $y>0$. We assume at time $t=0$, the tip of the body at the cross section of $z=0$ will pass the origin of the coordinate system. The wedge part of the body surface can then be written as

$$y=-(x-Ut)\tan\gamma_1 \tag{2}$$

in which, γ_1 is the half inner angle of the wedge, which is assumed to remain unchanged in the z direction. At each cross section where z is a constant, the tip of the wedge $(x \to Ut, y \to 0)$ is replaced by part of an ellipse. Its shape can be written as

$$(x-Ut+bz)^2+(cy)^2=(ez)^2 \tag{3}$$

in which b, c and e are constants. This equation shows that the major and minor axes of the

ellipse at each cross section changes with z, starting from zero at $z=0$. The two surfaces in Eqs (2) and (3) will form an intersection line on which we shall ensure that the normal of the surface is continuous. On the intersection line both Eqs (2) and (3) are satisfied. Replacing y in Eq.(3) with Eq.(2), we have

$$(1+c^2\tan^2\gamma_1)(x-Ut)^2+2bz(x-Ut)+(b^2-e^2)z^2=0 \tag{4}$$

We consider the cross section at each given z. Within this section, the slope of the curve on the wedge part can be written as

$$\frac{dy}{dx}=-\tan\gamma_1 \tag{5}$$

while the slope on the ellipse side is

$$\frac{dy}{dx}=\frac{x-Ut+bz}{c^2(x-Ut)\tan\gamma_1} \tag{6}$$

Equating Eqs (5) and (6) to ensure the continuity at the intersection, we have

$$(1+c^2\tan^2\gamma_1)(x-Ut)=-bz \tag{7}$$

This then means a line L can be taken at the intersection, which can be tangential to both sides. Substitution of Eq. (7) into Eq. (4) gives

$$x-Ut=-\frac{(b^2-e^2)}{b}z \tag{8}$$

Comparing the coefficients of Eqs (7) and (8), we have

$$\tan^2\gamma_1=\frac{e^2}{c^2(b^2-e^2)} \tag{9}$$

Combination of this equation with Eq.(2) means that the intersection of the two surfaces is a straight line. The cross product of this line and the line L mentioned in Eq.(8) can give the normal direction of the surface, which are continuous at the intersection. With the above body configuration, and the impermeable boundary condition for the velocity potential, we have on the body surface

$$\partial\phi/\partial n=Un_x \tag{10}$$

where $\mathbf{n}=(n_x,n_y,n_z)$ with

$$\begin{cases} n_x=\sin\gamma_1,\ n_y=\cos\gamma_1, & x-Ut<-(b^2-e^2)z/b \\ n_x=\dfrac{x-Ut+bz}{A},\ n_y=\dfrac{c^2y}{A},\ n_z=\dfrac{b(x-Ut)+(b^2-e^2)z}{A}, & x-Ut\ge-(b^2-e^2)z/b \\ A=\sqrt{(x-Ut+bz)^2+(c^2y)^2+[b(x-Ut)+(b^2-e^2)z]^2} \end{cases} \tag{11}$$

If we let n_x, n_y, n_z in the second line approach the intersection, we can confirm that the normal tends to that in the first line, or the normal is continuous. The undisturbed free surface can be written as

$$z=x\tan\gamma_2 \tag{12}$$

in which γ_2 is the angle between the beach surface and the horizontal plane. On the disturbed free surface, the kinematic and dynamic boundary conditions on the space fixed coordinate system $O-xyz$ can be respectively written as

$$\zeta_t = \phi_z - \zeta_x\phi_x - \zeta_y\phi_y \tag{13}$$

$$\phi_t = -\frac{1}{2}\left(\phi_x^2 + \phi_y^2 + \phi_z^2\right) \tag{14}$$

in which $z = \zeta(x, y)$. On the beach surface, we have

$$\frac{\partial\phi}{\partial n} = 0, \qquad z = 0 \tag{15}$$

Far away from the body, the fluid is assumed to be undisturbed and thus we have

$$\phi \to 0, \qquad \sqrt{x^2 + y^2 + z^2} \to 0 \tag{16}$$

2.2. Self-similar solution

The distance $s = Ut$ that the body has travelled along the beach is used as the length scale. A stretched coordinate system together with the corresponding potential φ can be defined as

$$x = s\bar{x}\ ,\quad y = s\bar{y}\ ,\quad z = s\bar{z}\ ,\quad \phi = sU\varphi \tag{17}$$

The body constructed in the previous section is in fact based on a combination of a wedge and an elliptical cone. During water entry of each of these bodies separately, the generated free surface flow may be self-similar when the gravity effect is ignored. Here we verify that the self-similar solution, in which φ and $\bar{\zeta} = \zeta / s$ are not explicitly a function of s in the stretched coordinate system, can be possible when a wedge and cone are combined. The Laplace equation, the beach surface condition in Eq.(15) and the far field boundary condition in Eq.(16) clearly retain their forms and do not contain s in the stretched coordinate system. The shape of the body surface can be written as

$$\begin{cases} \bar{y} = -(\bar{x} - 1)\tan\gamma_1, & \bar{x} - 1 < -(b^2 - e^2)\bar{z} / b \\ (\bar{x} - 1 + b\bar{z})^2 + (c\bar{y})^2 = (e\bar{z})^2, & \bar{x} - 1 \ge -(b^2 - e^2)\bar{z} / b \end{cases} \tag{18}$$

The body surface boundary condition in Eqs (10) and (11) can be respectively written as

$$\partial\varphi / \partial n = n_{\bar{x}} \tag{19}$$

$$\begin{cases} n_{\bar{x}} = \sin\gamma_1,\ n_{\bar{y}} = \cos\gamma_1, & \bar{x} - 1 < -(b^2 - e^2)\bar{z} / b \\ n_{\bar{x}} = \dfrac{\bar{x} - 1 + b\bar{z}}{\bar{A}},\ n_{\bar{y}} = \dfrac{c^2\bar{y}}{\bar{A}},\ n_{\bar{z}} = \dfrac{b(\bar{x} - 1) + (b^2 - e^2)\bar{z}}{\bar{A}}, & \bar{x} - 1 \ge -(b^2 - e^2)\bar{z} / b \\ \bar{A} = \sqrt{(\bar{x} - 1 + b\bar{z})^2 + (c^2\bar{y})^2 + [b(\bar{x} - 1) + (b^2 - e^2)\bar{z}]^2} \end{cases} \tag{20}$$

The free surface boundary conditions in Eqs (13) and (14) can be written as

$$\bar{\zeta} - \bar{x}\bar{\zeta}_{\bar{x}} - \bar{y}\bar{\zeta}_{\bar{y}} = \varphi_{\bar{z}} - \bar{\zeta}_{\bar{x}}\varphi_{\bar{x}} - \bar{\zeta}_{\bar{y}}\varphi_{\bar{y}} \tag{21}$$

$$\varphi - \bar{x}\varphi_{\bar{x}} - \bar{y}\varphi_{\bar{y}} - \bar{z}\varphi_{\bar{z}} = -\frac{1}{2}\left(\varphi_{\bar{x}}^2 + \varphi_{\bar{y}}^2 + \varphi_{\bar{z}}^2\right) \tag{22}$$

It can be seen that none of the above equations contain s explicitly. Therefore self-similar solution can be expected for this body geometry.

If we redefine s in Eq.(17) as

$$s = Ut\tan\gamma_2 \tag{23}$$

In the body fixed coordinate system $O'-x'y'z'$, Eqs (21) and (22) can be written as

$$(\zeta' - x'\zeta'_{x'} - y'\zeta'_{y'})\tan\gamma_2 = \varphi_{z'} - \zeta'_{x'}(\varphi_{x'} - 1) - \zeta'_{y'}\varphi_{y'} \tag{24}$$

$$(\varphi - x'\varphi_{x'} - y'\varphi_{y'} - z'\varphi_{z'})\tan\gamma_2 = \varphi_{x'} - \frac{1}{2}\left(\varphi_{x'}^2 + \varphi_{y'}^2 + \varphi_{z'}^2\right) \tag{25}$$

in which $x' = \bar{x} - 1/\tan\gamma_2$, $y' = \bar{y}$, $z' = \bar{z}$ and O' is located at the tip of the wedge cylinder. As $\gamma_2 \to 0$, or the beach tends to be horizontal, the left hand sides of Eqs (24) and (25) become zero and the two equations will be identical to the boundary conditions for the steady flow. The wedge is horizontal in such a case and extends to $x' \to -\infty$. Although this is not a typical ship of finite length, the result near the front of the body can capture some important features of the bow flow, as in the 2D case considered by Dias and Vanden-Broeck (1993).

2.3. The solution procedure through the boundary element method

Using Green's identity, the Laplace equation in fluid domain can be converted into an integral equation over the boundary with the Green function G. The potential at point p can be written as

$$A(p)\varphi(p) = \iint\left(G\frac{\partial\varphi(q)}{\partial n} - \varphi(q)\frac{\partial G}{\partial n}\right)ds_q \tag{26}$$

where $A(p)$ is the solid angle at point p. The Green function could be defined as $G = 1/R_{pq}$, where R_{pq} is the distance between points q and p. With such a definition, the integration in Eq.(26) is performed over the entire boundary of the fluid domain. We notice that on the planes $\bar{y} = 0$ and $\bar{z} = 0$, $\frac{\partial\varphi}{\partial n} = 0$ in this problem. Thus, if G is chosen as

$$\begin{aligned} G = &\frac{1}{\sqrt{(\bar{x}_q - \bar{x}_p)^2 + (\bar{y}_q - \bar{y}_p)^2 + (\bar{z}_q - \bar{z}_p)^2}} + \frac{1}{\sqrt{(\bar{x}_q - \bar{x}_p)^2 + (\bar{y}_q + \bar{y}_p)^2 + (\bar{z}_q - \bar{z}_p)^2}} \\ &+ \frac{1}{\sqrt{(\bar{x}_q - \bar{x}_p)^2 + (\bar{y}_q - \bar{y}_p)^2 + (\bar{z}_q + \bar{z}_p)^2}} + \frac{1}{\sqrt{(\bar{x}_q - \bar{x}_p)^2 + (\bar{y}_q + \bar{y}_p)^2 + (\bar{z}_q + \bar{z}_p)^2}} \end{aligned} \tag{27}$$

it also satisfies $\frac{\partial G}{\partial n} = 0$ on both $\bar{y} = 0$ plane and $\bar{z} = 0$ plane. As a result, the integration in Eq.(26) needs to be performed only on body surface, free surface and far field surface, with $\bar{y} > 0$ and $\bar{z} > 0$.

The boundary element method is used to solve Eq.(26). The boundary is first divided into small quadrilateral elements and within each element the potential and its normal derivative are assumed to vary linearly.

$$\mathbf{r} = \bar{x}\mathbf{i} + \bar{y}\mathbf{j} + \bar{z}\mathbf{k} = \sum_{k=1}^{K} h_k(\mu,\nu)\mathbf{r}_k \tag{28}$$

$$\varphi = \sum_{k=1}^{K} h_k(\mu,\nu)\varphi_k \ , \quad \frac{\partial \varphi}{\partial n} = \sum_{k=1}^{K} h_k(\mu,\nu)\frac{\partial \varphi}{\partial n}_k \tag{29}$$

in which, K=4 is the total number of the nodes in each element, h_k are the shape functions. μ and ν are the local intrinsic coordinates and $\mathbf{r}$ is the position vector from the origin. The shape function h_k can be chosen as

$$\begin{aligned} h_1 &= \frac{1}{4}(1+\mu)(1+\nu), \quad h_2 = \frac{1}{4}(1-\mu)(1+\nu) \\ h_3 &= \frac{1}{4}(1-\mu)(1-\nu), \quad h_4 = \frac{1}{4}(1+\mu)(1-\nu) \end{aligned} \tag{30}$$

where $-1 \le \mu \le 1$ and $-1 \le \nu \le 1$. Discretizing the whole boundary in Eq.(26) into N_E quadrilateral elements and substituting Eqs (28) and (29) into Eq.(26), we obtain

$$\begin{aligned} A(p)\varphi(p) = &\sum_{n=1}^{N_E}\int_{-1}^{1}\int_{-1}^{1} G\sum_{k=1}^{K} h_k(\mu,\nu)\frac{\partial \varphi}{\partial n}_k \ J_n(\mu,\nu)d\mu d\nu \\ &- \sum_{n=1}^{N_E}\int_{-1}^{1}\int_{-1}^{1}\frac{\partial G}{\partial n}\sum_{k=1}^{K} h_k(\mu,\nu)\varphi_k J_n(\mu,\nu)d\mu d\nu \end{aligned} \tag{31}$$

where the Jacobian $J_n(\mu,\nu)$ is

$$J_n(\mu,\nu) = \sum_{k=1}^{K} h_k(\mu,\nu)c_k \tag{32}$$

and c_k is the modulus of the cross product of the vectors from node k to its two neighbouring nodes within the quadrilateral element. It ought to mention that the integration in Eq.(31) is performed for each element at a given n and the corresponding integrand is defined within this given element. The discretized integral equation (31) can be written in the following matrix form

$$[H]_{N_d \times N_d} \cdot [\varphi]_{N_d \times 1} = [M]_{N_d \times N_d} \cdot \left[\frac{\partial \varphi}{\partial n}\right]_{N_d \times 1} \tag{33}$$

in which, N_d is total number of nodes, H and M are respectively the matrixes obtained by integrating $\frac{\partial G}{\partial n}$ and G along the boundary. This equation can be used to obtain the unknown quantities on the boundaries.

The surface integrations in Eq.(31) can be performed using the Gauss integration with respect to the variable μ and ν directly when the field point p is not located at the element where the source point q is. When these two points p and q are on the same element, there is a singularity in the Green function and its normal derivative. To deal with that, integration of $\frac{\partial G}{\partial n}$ over the element is obtained through (Brebbia, 1978; Wang and Yeo, 1996)

$$H_{ii} = -\sum_{j=1,\, j\neq i}^{N_d} H_{ij} \tag{34}$$

For the singularity in G, let us assume that it exists at the node of $\mu = \nu = 0$. The integration will then have the form

$$\int_{-1}^{1}\int_{-1}^{1} \frac{f(\mu,\nu)}{R} d\mu d\nu \tag{35}$$

where $f(\mu,\nu)$ is regular at $\mu = \nu = 0$. Following the procedure of Telles (1987), we use the transformation $\mu = R\cos\theta$, $\nu = R\sin\theta$. Eq.(35) then becomes

$$\int_{0}^{2\pi}\int_{0}^{R(\theta)} f(\mu,\nu) dR d\theta \tag{36}$$

in which the singularity disappears.

For the self-similar problem, the boundary conditions on the free surface in Eqs (21) and (22) can be satisfied through iteration. It starts with an assumed potential on the free surface together with its shape. Once the solution of Eq.(26) is obtained through the BEM, the elevation of and the potential on the free surface can be updated through Eqs (21) and (22). Eq.(26) is then resolved and the process continues until the convergence has been achieved. This is the procedure used by Sun and Wu (2014) for a 3D water column impacting on a flat wall, in which Eqs (21) and (22) are imposed in an integral form. During the simulation, the elements may be distorted. As a result, the mesh may have to be regenerated regularly and the results from the old mesh have to be transferred to the new one (Sun and Wu, 2013a).

As the self-similar problem is a special case of the general transient problem, it can be also solved in the time domain. In the physical system, we can assume that the body has already been put into water with a small distance $s = s_0$ at the beginning of the simulation. The free surface at such a moment is assumed to be undisturbed and the potential on the water surface is zero. We should notice that s_0 can be chosen arbitrarily small and indeed at $s = s_0$ or any s subsequently, the tip of the body on the beach is always at $\bar{x} = 1$ in the stretched coordinate system. Eq.(26) can then be solved through BEM. In the stretched coordinate system, Eqs (13) and (14) can be written as

$$\frac{\partial s\bar{\zeta}}{\partial s} = \varphi_{\bar{z}} - \bar{\zeta}_{\bar{x}}\varphi_{\bar{x}} - \bar{\zeta}_{\bar{y}}\varphi_{\bar{y}} \tag{37}$$

$$\frac{\partial s\varphi}{\partial s} = -\frac{1}{2}\left(\varphi_{\bar{x}}^2 + \varphi_{\bar{y}}^2 + \varphi_{\bar{z}}^2\right) \tag{38}$$

They can be used to update the free surface and potential at the next time step. Eq.(26) is then solved again and the process continues with the time step until the desired stage (Sun and Wu, 2013a, 2013b). As in the iteration process for Eqs (21) and (22), the mesh may become distorted during the simulation and remeshing may have to be applied every several time steps. As s_0 can be chosen arbitrarily small, the assumption made at the initial stage does not have lasting effect for this problem. After a numerical transition period, the solution becomes physical. In particular, the

flow will tend to be self-similar for the present case, and the solution will tend to that obtained from the iteration method above. This in fact has been verified by Sun and Wu (2013a, 2013b) through a similar problem on water entry of 3D bodies.

It should be mentioned that the shape of the free surface in this case is highly complex. $\overline{\zeta}$ may not be always single valued. $\overline{\zeta}_{\bar{x}}$ or $\overline{\zeta}_{\bar{y}}$ in Eqs (37) and (38) can be very large or even tend to infinity. This can cause major difficulty in the numerical calculation. To solve this problem, a local coordinate system $O-\hat{x}\hat{y}\hat{z}$ is introduced, in which $\hat{z}$ is normal to the free surface, and $\hat{x}$ and $\hat{y}$ are in two tangential directions perpendicular to each other. In this coordinate system, we consider a point with fixed $\hat{x}$ and $\hat{y}$, or $\frac{\partial \hat{x}}{\partial s}=0$, $\frac{\partial \hat{y}}{\partial s}=0$, which can also be written as

$$\frac{\partial s\hat{x}}{\partial s}=\hat{x},\quad \frac{\partial s\hat{y}}{\partial s}=\hat{y} \tag{39}$$

The free surface elevation in the $\hat{z}$ direction can then be obtained from (Sun and Wu, 2013b)

$$\frac{\delta s\hat{\zeta}}{\delta s}-\hat{x}\hat{\zeta}_{\hat{x}}-\hat{y}\hat{\zeta}_{\hat{y}}=\varphi_{\hat{z}}-\hat{\zeta}_{\hat{x}}\varphi_{\hat{x}}-\hat{\zeta}_{\hat{y}}\varphi_{\hat{y}} \tag{40}$$

The potential at this newly elevated point can be obtained from

$$\frac{\delta s\varphi}{\delta s}-\hat{x}\varphi_{\hat{x}}-\hat{y}\varphi_{\hat{y}}-\frac{\delta s\hat{\zeta}}{\delta s}\varphi_{\hat{z}}=-\frac{1}{2}\left(\varphi_{\hat{x}}^2+\varphi_{\hat{y}}^2+\varphi_{\hat{z}}^2\right) \tag{41}$$

As $\hat{z}$ is in the local normal direction, we have $\hat{\zeta}_{\hat{x}}=0$ and $\hat{\zeta}_{\hat{y}}=0$, which avoids the difficulty due to extremely large derivative. On the intersection line between free surface and the body or beach, or the waterline, the wave elevation should move along the body surface. Especially on the intersection line between the flat wedge surface and the smooth ellipse front, $\hat{z}$ should be along this intersection line to ensure that the wave elevation is along this intersection, which can improve the performance of the numerical simulation.

When the solution of Eq.(26) is found at each given time step, the pressure can be obtained from the Bernoulli equation

$$p=-\rho(\phi_t+\frac{1}{2}\nabla\phi\cdot\nabla\phi) \tag{42}$$

in which, $\nabla\phi$ can be found directly once the potential has been obtained. For the general transient problem, the term ϕ_t in Eq. (42) cannot be obtained directly from the potential at this particular instant. Here we adopt the procedure which treats it as another harmonic function satisfying the Laplace equation. On the free surface, $p=0$ gives

$$\phi_t=-\frac{1}{2}\left(\phi_x^2+\phi_y^2+\phi_z^2\right) \tag{43}$$

On the body surface, we have (Wu, 1998)

$$\frac{\partial\phi_t}{\partial n}=-U\frac{\partial\phi_x}{\partial n} \tag{44}$$

We may define $U^2\chi(\bar{x},\bar{y},\bar{z}) = \phi_t(x,y,z)$ and $\chi = -\varphi_{\bar{x}} + \chi_1$ (Wu et al., 2004). Obviously χ_1 satisfies the Laplace equation. On the body surface, we have

$$\frac{\partial \chi_1}{\partial n} = 0 \tag{45}$$

and on the free surface, Eq. (43) gives

$$\chi_1 = -\frac{1}{2}\nabla\varphi\cdot\nabla\varphi + \varphi_{\bar{x}} \tag{46}$$

The condition at the control surface at the far field can be written as

$$\chi_1 = 0 \tag{47}$$

The solution of χ_1 can be then found in a manner similar to that used for φ and the pressure can be obtained from the following equation

$$C_p = p/(\rho U^2/2) = -(2\chi_1 - 2\varphi_{\bar{x}} + \nabla\varphi\cdot\nabla\varphi) \tag{48}$$

For the self-similar problem, the pressure coefficient can be obtained directly from

$$C_p = \frac{p}{\rho U^2/2} = -(2\varphi - 2\bar{x}\varphi_{\bar{x}} - 2\bar{y}\varphi_{\bar{y}} - 2\bar{z}\varphi_{\bar{z}} + \nabla\varphi\cdot\nabla\varphi) \tag{49}$$

The force coefficient in the x direction can be obtained by integrating the pressure C_p along body surface

$$C_f^x = \int C_p n_x ds \tag{50}$$

3. Numerical results and discussions

The fluid boundary in the present case includes the body surface which is in fact a combination of a vertical wedge and an elliptical cone, and the free surface which will become curved and highly distorted as the body slides into water. To generate mesh for such a complex boundary using boundary elements is always a challenging task. This is further complicated by the fact the boundary changes or deforms during the simulation and the mesh has to be regenerated regularly. Here at the start of the simulation $s = s_0$, the waterline of the body surface is divided into N_a segments. Each of these nodes are then linked with the body tip on the beach ($\bar{x} = 1$, $\bar{y} = 0$, $\bar{z} = 0$) to form N_a lines, one of which corresponds to line L defined in Eq. (8). These lines will then intersect with N_b lines at different $\bar{z}$ to form a mesh on the body surface. Using the nodes on the waterline of the body, N_a lines are drawn in the radial direction of the free surface, varying from the waterline of the beach along the x axis to the y axis. N_c lines will then be drawn along the circumferential direction to form mesh on the free surface. As the simulation continues, all these lines will be curved in the 3D space. This causes some major difficulty in remeshing and interpolation. Here we follow the procedure in Sun and Wu (2013a, 2013b). The element nodes along the lines in the radial direction of the free surface are redistributed during the simulation. Taking the waterline of the beach for example, the smallest segment length d is used near the jet

root. Away from the jet root, the element size increases at a fixed ratio r. Assuming that the length of the first mesh line is $l(1)$ and the arc length of node n is s_n, then for the i^{th} line of length $l(i)$ in the radial direction, the arc length of the node n will be $s_n \cdot l(i)/l(1)$. The n^{th} node of each line along the radial direction will be linked together in the circumferential direction and a new mesh will be generated.

A solid block with $\gamma_1 = \pi/6$, $e/b = 0.8$ and $b = 1$ sliding along a beach with inclined angle $\gamma_2 = \pi/6$ is used to show how results from the present simulation evolve into self-similar flow and how the results become convergent with respect to time step and element size. The far field control surface is taken at $\sqrt{\bar{x}^2 + \bar{y}^2 + \bar{z}^2} = 10$, which has been found to be sufficiently far. The free surface elevations in $O - \alpha\bar{y}\beta$ system at different time are given in Fig.2 through s/s_0, in which the red part is the wetted surface of the body, the blue part is the free surface, the grey part is the beach, $\alpha = \bar{x}\cos\gamma_2 + \bar{z}\sin\gamma_2$ is along the free surface and $\beta = -\bar{x}\sin\gamma_2 + \bar{z}\cos\gamma_2$ is perpendicular to the free surface. The simulation starts at $s = s_0$ at which the free surface is taken as flat. It can be seen from the figures that the water surface from the simulation climes quickly along the body surface and the beach surface when s/s_0 is relatively smaller. In particular, the free surface deforms significantly. The variation of the wetted surface and the deformation of the free surface slow down in the stretched coordinate system, as s/s_0 increases or the time increases. These changes then diminish and the results become stable at $s/s_0 \approx 5$. This shows that the problem is no longer time dependent in the stretched coordinate system and it has become self-similar. In Fig.3, the pressures along transverse sections $\bar{z} = 0.3$ and $\bar{z} = 0.6$ at different time s/s_0 are given. Similar to the variation of free surface, there is a numerical transition period. At the initial time step, or $s/s_0 = 1$, the pressure of $\bar{z} = 0.3$ near the free surface is very large and negative. The result gradually tends to a stable value as s/s_0 increases.

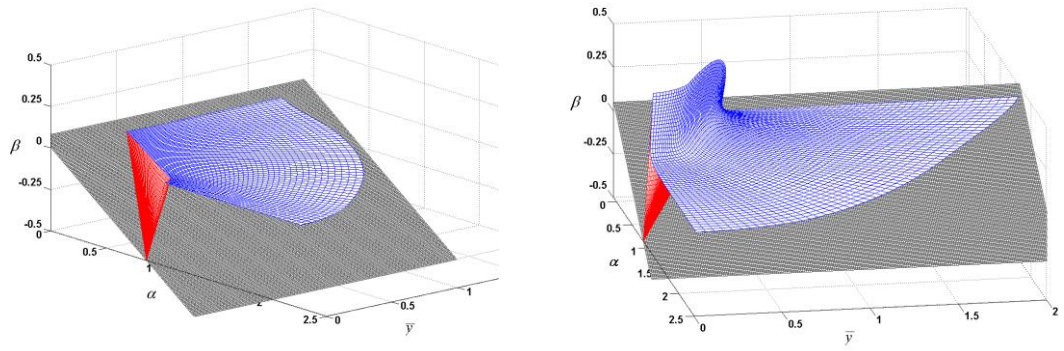

(a) (b)

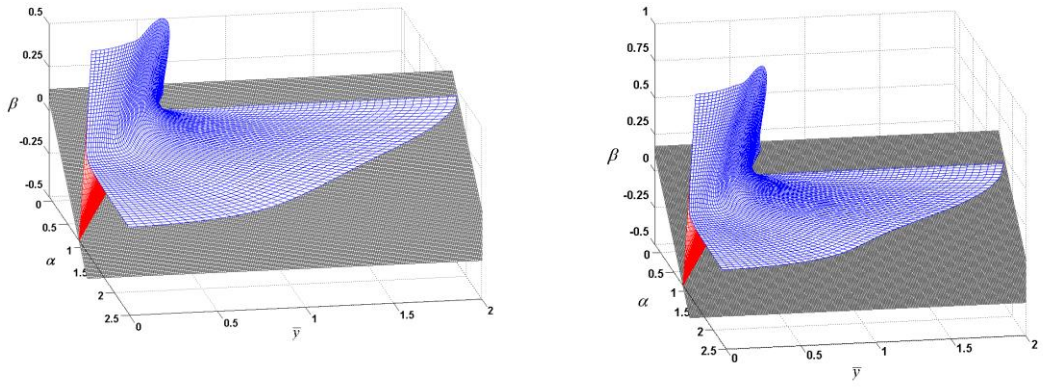

(c) (d)

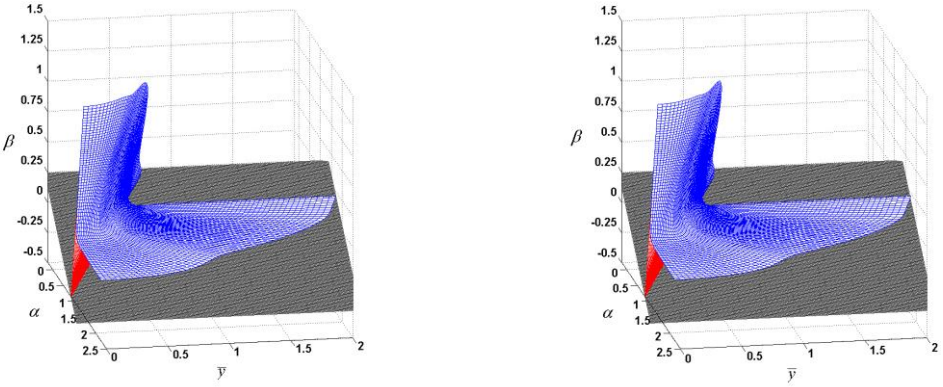

(e) (f)

Fig.2. Free surface elevation at different time s/s_0, (a) $s/s_0=1$, (b) $s/s_0=1.3$, (c) $s/s_0=1.6$, (d) $s/s_0=2$, (e) $s/s_0=3$, (f) $s/s_0=5$.

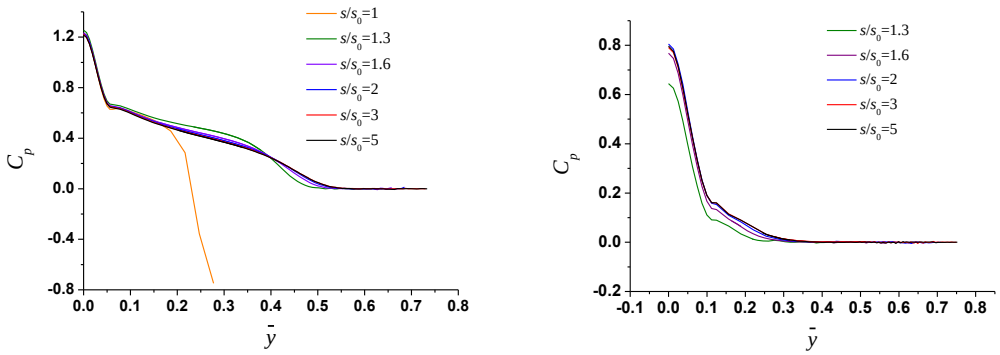

(a) (b)

Fig.3. Pressure at different time s/s_0, (a) $\bar{z}=0.3$, (b) $\bar{z}=0.6$.

The pressure distribution along three representative lines, or the intersection line between the body and beach, the intersection line L between the wedge and the elliptical cone, and the intersection line between the body and $\bar{y}=0$ plane, are given in Figs 4(a), 4(b) and 4(c). It can be seen that the curves for pressure on the solid block from different meshes and time steps are graphically indistinguishable. This means that the present results have converged with respect to time step and element size.

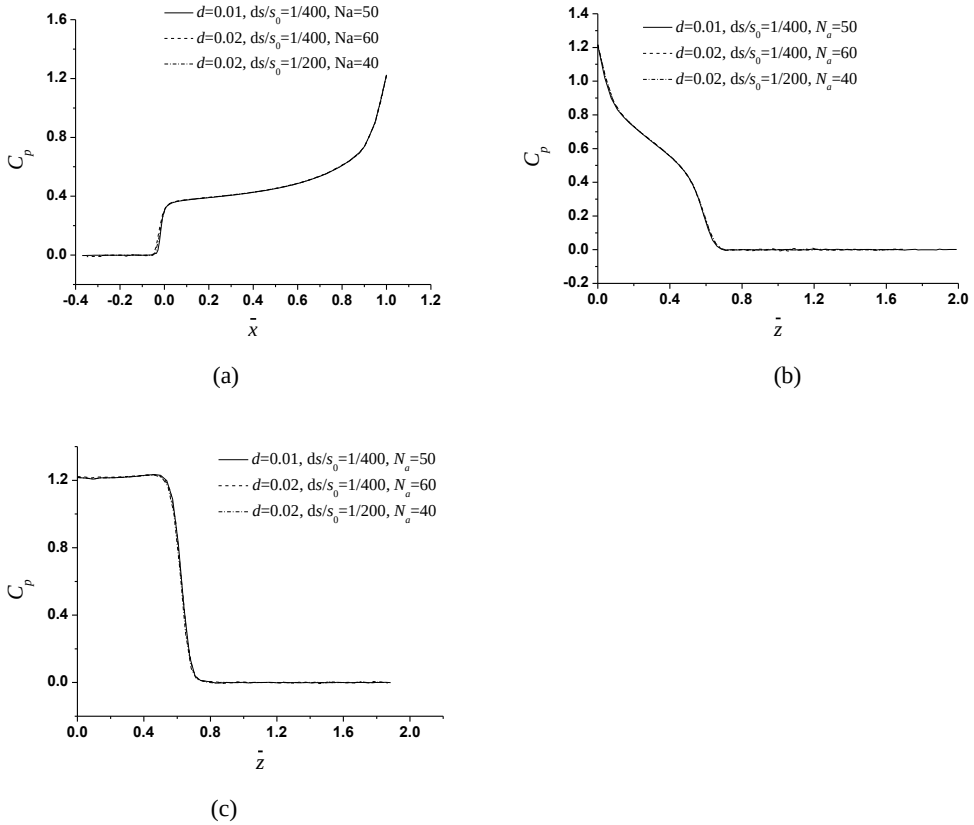

Fig.4. Convergence study through pressure distribution, (a) The intersection line between the body and the beach surfaces ($\bar{z}=0$), (b) The intersection line L between the wedge and the elliptical cone (see Eq.(8)), (c) The intersection line between the body and $\bar{y}=0$ plane. d in the figure denotes the size of the element at the jet root of the waterline of the beach.

More detailed results for the body in Fig.2 are provided in Fig.5, at $\bar{z}=0$, $\bar{z}=0.1$, $\bar{z}=0.2$, $\bar{z}=0.3$, $\bar{z}=0.4$, $\bar{z}=0.5$, $\bar{z}=0.6$ respectively. The projections of these cross sections, the undisturbed waterline and the disturbed waterline onto $O-\bar{x}\bar{y}$ plane are shown in Fig.5(a), while the pressures at these sections are given in Fig.5(b). The figure shows that the peak pressure is at $\bar{y}=0$ for all these sections, and its value is around 1.2 when $\bar{z}\le 0.5$. At $\bar{z}=0.6$, the peak pressure at $\bar{y}=0$ suddenly decreases to around 0.8, which indicates a large local pressure gradient in the $\bar{z}$ direction. This in fact can be seen in Fig.4(c). It shows that the pressure is nearly constant when $\bar{z}\le 0.5$. After that the pressure experiences a sharp decrease. The reason for that is that $\bar{z}=0.6$ is near the undisturbed free surface. When the fluid particle on the free surface moves towards the body, its path is blocked and has to move upwards. This leads to a large acceleration and therefore a large pressure gradient in the $\bar{z}$ direction. In Fig.5(b), we also notice a large pressure gradient in the $\bar{y}$ direction near $\bar{y}=0$. This is because the incoming flow towards the body has to bend itself to move along the body surface direction, leading to a large acceleration and thus large pressure gradient. When $\bar{z}$ increases, the curvature of body front along $O-\bar{x}\bar{y}$ plane will become smaller and thus the pressure variation there with $\bar{y}$ will also become smaller.

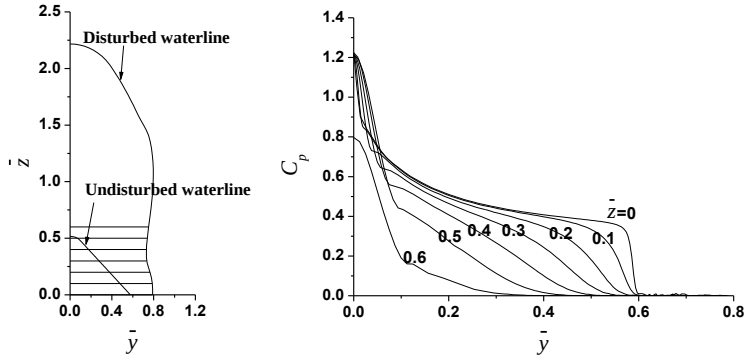

(a) (b)

Fig.5. A solid block of $\gamma_1=\pi/6$, $e/b=0.8$, $b=1$ sliding along a beach of $\gamma_2=\pi/6$ into water, (a) Projection of cross sections of constant $\bar{z}$ onto $O-\bar{y}\bar{z}$ plane, (b) Pressure distribution along the lines of constant $\bar{z}$.

Further results are provided in Figs 6 and 7 for the cases with the same b, γ_1 and γ_2 as above but different body fronts of $e/b=0.7$, 0.8 and 0.9. The variation of the pressures with the front shape at a fixed $\bar{z}$ are given through $\bar{z}=0.2$ and 0.4 in Figs 6(b) and 7(b) respectively. These figures show that the local variation of the front does not have too much overall effect on the pressure distribution. Figs 6(a) and 7(a) show that as e/b increases the front of the cross section at given $\bar{z}$ becomes less blunt. A less blunt front, however, corresponds to a larger local pressure variation, as shown in Figs 6(b) and 7(b). This is similar to what was observed in Wu and Sun (2014) for water entry of an expanding paraboloid, where the explanation for such behaviour is given. Along the body front line itself, or the intersection line between the body and $\bar{y}=0$ plane as shown in Fig.8(a), the pressure distribution for different e/b is given in Fig.8(b). All the pressures are close to each other at the body tip ($\bar{x}=1$). We should notice that this point corresponds to $\bar{z}=0$. The cross section at $\bar{z}=0$, or on the beach, is always a triangle, which does not change with e/b. Away from that point the pressure is significantly affected by the variation of e/b.

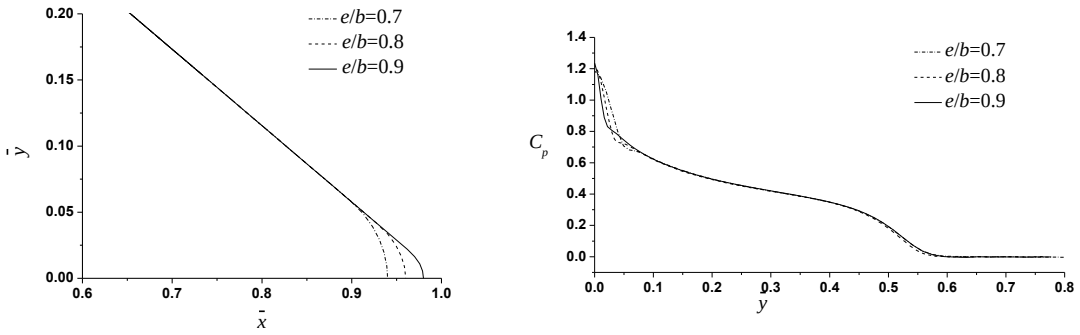

(a) (b)

Fig.6. The intersection line of the body cross section with $\bar{z}=0.2$ and pressure distribution along the intersection line at different e/b. (a) Body cross section shape, (b) Pressure.

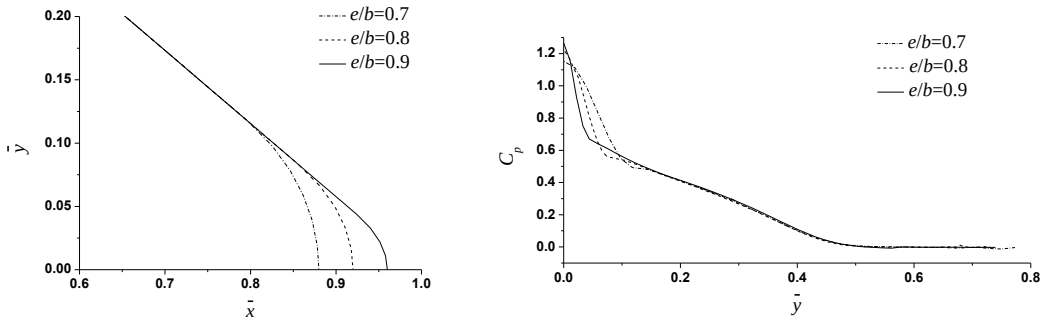

(a) (b)

Fig.7. The intersection line of the body cross section with $\bar{z} = 0.4$ and pressure distribution along the intersection line at different e/b. (a) Body cross section shape, (b) Pressure.

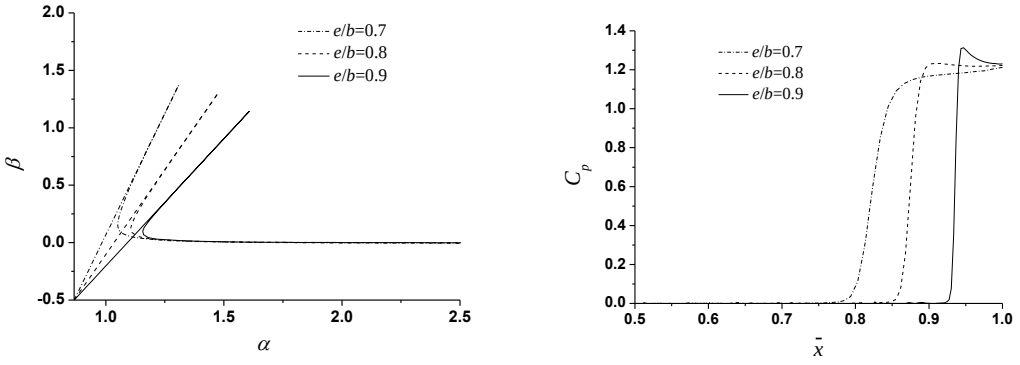

(a) (b)

Fig.8. The intersection line between the body and $\bar{y} = 0$ plane and pressure distribution. (a) Free surface elevation, (b) Pressure.

We now consider the case of a given solid block with $\gamma_1 = \pi/6$, $e/b = 0.8$ and $b = 1$ sliding along beaches of different angles. The pressure distributions on the body surface at $\bar{z} = 0.2$ and 0.4 are given in Fig.9 for $\gamma_2 = \pi/3, \pi/4$ and $\pi/6$. We notice that at small γ_2 the plane of constant $\bar{z}$ tends to be horizontal while at large γ_2 the plane tends to be vertical. The latter is expected to experience larger impact force. Thus Fig.9 shows that the pressure at larger γ_2 is bigger than that at smaller γ_2. In Fig.10(a), the free surface elevation in the $\bar{y} = 0$ plane is given while in Fig.10(b) the pressure distribution along the intersection of the $\bar{y} = 0$ plane and the body surface is provided. Larger γ_2 corresponds to a smaller deadrise angle, or the angle between the intersection line with $\bar{y} = 0$ plane and the undisturbed free surface. Thus the pressure increases significantly. In particular, similar to other impacts at small deadrise angle, the location of the peak pressure has moved from the tip to the jet root, as the fluid particles need to take a larger turn locally. Figs 11(a) and 11(b) show the pressure along the line L defined in

Eq.(8) and the intersection line between the body and the beach surface ($\bar{z}=0$) respectively. For these two lines, the peak pressure is at the body tip ($\bar{x}=1, \bar{z}=0$), and the pressure deceases along the line from body tip to the waterline. The total force coefficient in the $\bar{x}$ direction is given in Table 1.

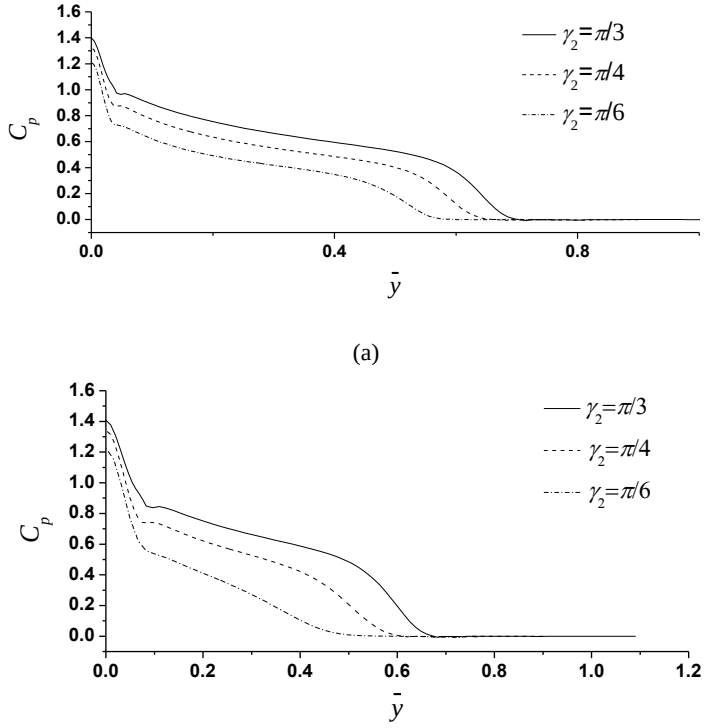

(a)

(b)

Fig.9. The pressure, $\gamma_1=\pi/6$, $e/b=0.8$, $b=1$. (a) $\bar{z}=0.2$, (b) $\bar{z}=0.4$.

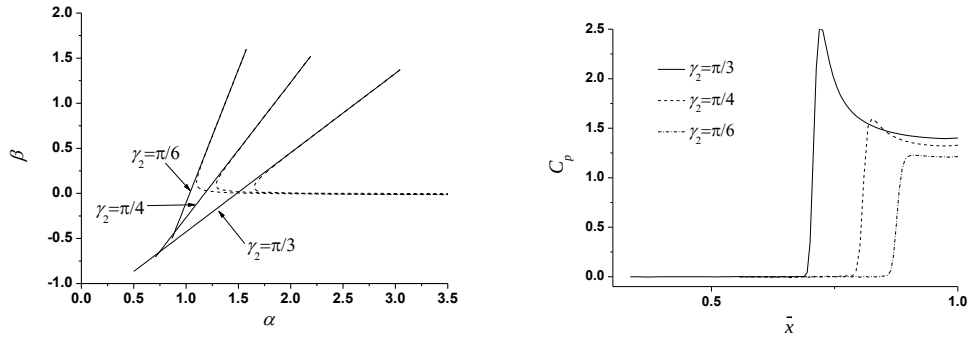

(a) (b)

Fig.10. Wave elevation and pressure on intersection of the body and $\bar{y}=0$ plane, (a) The free surface elevation, (b) Pressure.

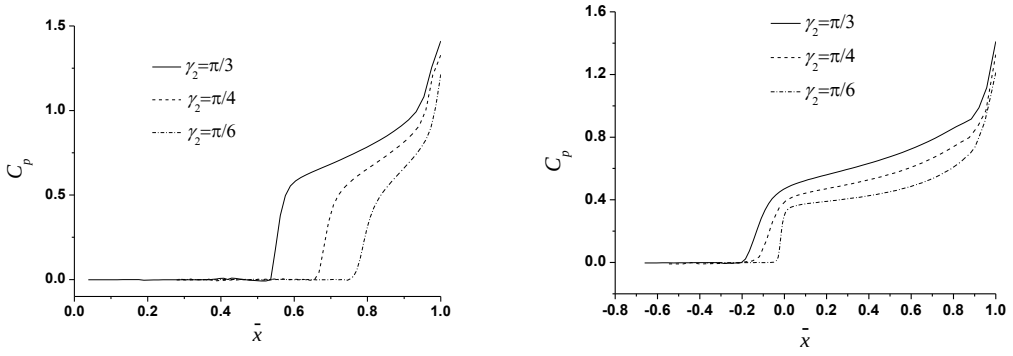

(a) (b)

Fig.11. The pressure along (a) the line L defined in Eq.(8) and (b) the intersection line between the body and the beach surface ($\bar{z}=0$).

Table 1 Force coefficient ($\gamma_1=\pi/6$)

γ_2	$\pi/3$	$\pi/4$	$\pi/6$
C_f^x	0.545	0.273	0.131

Figs 12(a) and 12(b) give the pressures at $\bar{z}=0.2$ and $\bar{z}=0.4$ respectively, on bodies of different inner angle γ_1 sliding on a beach of $\gamma_2=\pi/4$. The body will become blunter when the inner angle γ_1 increases. The pressure will increase significantly and its peak will move from the front of the body to the jet root where the flow takes a shape turn. The resultant force C_f^x is given in Table 2.

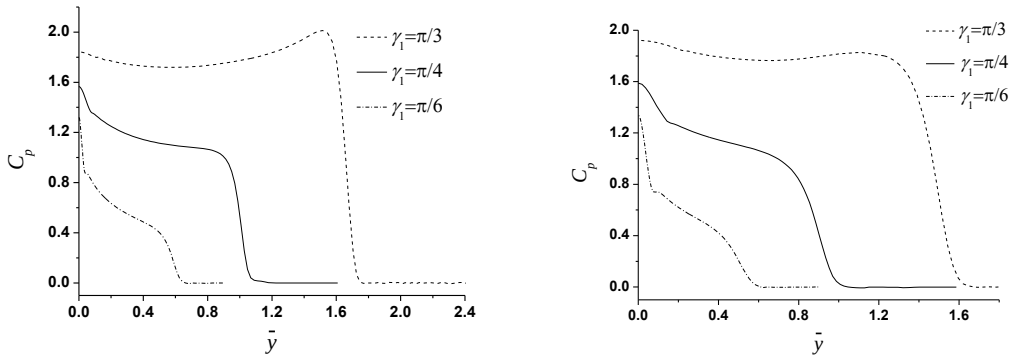

(a) (b)

Fig.12. The pressure at different γ_1 (e/b=0.8 , $b=1$, $\gamma_2=\pi/4$). (a) $\bar{z}=0.2$, (b) $\bar{z}=0.4$.

Table 2 Force coefficient ($\gamma_2=\pi/4$)

γ_1	$\pi/3$	$\pi/4$	$\pi/6$
C_f^x	2.728	0.929	0.273

4. Conclusions

Water entry of a 3D solid block along an inclined flat beach has been analysed based on the

velocity potential theory with the fully nonlinear boundary conditions, using the boundary element method. It has been demonstrated that the flow can be self-similar when the body is a combination of an infinite wedge and an elliptical cone. Method has been developed to overcome the difficulties in mesh generation and its regeneration during the simulation, which becomes highly complex due to the distortion of the free surface. Studies have been undertaken to show that the results have converged with respect to both time step and element size. The numerical results obtained show that although the shape of the elliptical front of the body does not have too much overall effect on the pressure distribution, the pressure along body front line changes significantly with the variation of the front shape. For a less blunt body with a smaller inner angle, pressure along the cross section perpendicular to the body axis is smaller. However, it also corresponds to a larger local pressure gradient near the front. The peak pressure may occur at the body front where flow bifurcation occurs, or the relative incoming flow along the symmetry line will split and move along the both sides of the body. However, as the problem resembles that of water entry impact or bow wave, depending on the inner angle of the body and inclination angle of the beach, very large local pressure and pressure gradient can occur where the flow direction bends suddenly, especially at the jet root. The present work is one step forward for the highly complex 3D fluid/structure impact problem. Further work is required for more general cases, such as to include the free surface breaking and secondary impact.

Acknowledgements

This work is supported by Lloyd's Register Foundation (LRF) through the joint centre involving University College London, Shanghai Jiaotong University and Harbin Engineering University, to which the authors are most grateful. LRF supports the advancement of engineering-related education, and funds research and development that enhances safety of life at sea, on land and in the air. This work is also supported by the National Natural Science Foundation of China (Grant No. 11472088 and 11302057).

References

Brebbia, C.A., 1978. The boundary element method for engineers. Pentech Press, London, UK.

Dagan, G., Tulin, M.P., 1972. Two-dimensional gravity free-surface flow past blunt bodies. Journal of Fluid Mechanics 51, 529-543.

Dias, F., Vanden-Broeck, J.-M., 1993. Nonlinear bow flows with spray. Journal of Fluid Mechanics 55, 91-102.

Dobrovol'Skaya, Z.N., 1969. On Some problems of similarity flow of fluid with a free surface. Journal of Fluid Mechanics 36, 805–829.

Hong, N., 2012. The melting Arctic and its impact on China's maritime transport. Research in Transportation Economics 35, 50-57.

Iafrati, A., 2013. A fully nonlinear iterative solution method for self-similar potential flows with a free boundary. Computer Methods in Applied Mechanics and Engineering 1-41. arXiv:1212.6699v2 [physics.flu-dyn].

Iafrati, A., Miloh, T., Korobkin, A., 2007. Oblique Water Entry of a Block Sliding along a Sloping Beach.In: Proceedings of International Conference on Violent Flows (VF-2007), Organized by RIAM, Kyushu University, Fukuoka, Japan, 1-9.

Hong, N., 2012. The melting Arctic and its impact on China's maritime transport. Research in Transportation Economics 35, 50-57.

Korobkin, A.A., Scolan, Y.M., 2006. Three-dimensional theory of water impact. Part 2.Linearized Wagner problem.Journal of Fluid Mechanics 549, 343–374.

Larsson, L., Baba, E., 1996. Ship resistance and flow computations. Advances in Marine Hydrodynamics5, 1–75.

Liu, P.L.-F., Wu, T.R., Raichlen, F., Synolakis, C.E., Borrero, J.C., 2005. Runup and rundown generated by three-dimensional sliding masses. Journal of Fluid Mechanics 536, 107-144.

Miloh, T., 1991. On the oblique water-entry problem of a rigid sphere.Journal of Engineering mathematics 25, 77-92.

Moore, M.R., Howison, S.D., Ockendon, J.R., Oliver, J.M., 2012. Three-dimensional oblique water-entry problems at small deadrise angle. Journal of Fluid Mechanics 711, 259-280.

Scolan, Y.M., Korobkin, A.A., 2001. Three-dimensional theory of water impact, Part 1: Inverse Wagner problem. Journal of Fluid Mechanics 440, 293-326.

Semenov, Y.A., Iafrati, A., 2006. On the nonlinear water entry problem of asymmetric wedges. Journal of Fluid Mechanics 547, 231–256.

Semenov, Y.A., Wu, G.X., 2013. Asymmetric impact between liquid and solid wedges. Proceedings of the Royal Society A, 469, 1-20.

Smith, L.C., Stephenson, S.R., 2013. New Trans-Arctic shipping routes navigableby midcentury. Proceedings of the National Academy of Sciences of the United States of America 110, 1191-1195.

Shakeri, M., Tavakolinejad, M., Duncan, J.H., 2009. An experimental investigation of divergent bow waves simulated by a two-dimensional plus temporal wave marker technique. Journal of Fluid Mechanics 634, 217–243.

Sun, S.L., Wu, G.X., 2013a. Oblique water entry of a cone by a fully three dimensional nonlinear method. Journal of Fluids and Structures 42, 313-332.

Sun, S.L., Wu, G.X., 2013b. Oblique water entry of non-axisymmetric bodies at varying speed by a fully nonlinear method. Quarterly Journal of Mechanics and Applied Mathematics 66, 366-393.

Sun, S.L., Wu, G.X., 2014. Self-similar solution for oblique impact of a water column with sharp front on a wall and its zero inner angle steady limit. Physics of Fluids 26, 082106, 1-17.

Synolakis, C.E., Liu, P.L.-F., Yeh, H., Carrier, G., 1997. Tsunamigenic seafloor deformations. Science 278, 598-600.

Telles, J.C.F., 1987. A self-adaptive co-ordinate transformation for efficient numerical evaluation of general boundary element integrals. International Journal for Numerical Methods in Engineering 24, 959-973.

Wang, Q.X., Yeo, K.S., Khoo, B.C., Lam, K.Y., 1996. Strong interaction between a buoyancy bubble and a free Surface. Theorectical and Computational Fluid Dynamics 8, 73-88.

Wu, G.X., 1998. Hydrodynamic force on a rigid body during impact with liquid. Journal of Fluids and Structures 12, 549-559.

Wu, G.X., Sun, H., He, Y.S., 2004. Numerical simulation and experimental study of water entry of a wedge in free fall motion. Journal of Fluids and Structures 19, 277-289.

Wu, G.X., Sun, S.L., 2014. Similarity solution for oblique water entry of an expanding paraboloid. Journal of Fluid Mechanics 745, 398-408.

Xu, G.D., Duan, W.Y., Wu, G.X., 2010. Simulation of water entry of a wedge through free fall in three degrees of freedom. Proceedings of the Royal Society A 466, 2219-2239.

Zhao, R., Faltinsen, O., 1993. Water entry of two-dimensional bodies. Journal of Fluid Mechanics 246, 593–612.

Zweifel, A., Hager, W.H., Minor H.-E., 2006. Plane Impulse Waves in Reservoirs. Journal of Waterway, Port, Coastal, and Ocean Engineering 132, 358-368.